An Efficient Parameterization of Convective and Nonconvective Planetary Boundary Layers for Use in Numerical Models

SIMON WEI-JEN CHANG

JAYCOR, 205 S. Whiting Street, Alexandria, VA 22304

(Manuscript received 14 July 1978, in final form 21 May 1979)

ABSTRACT

An efficient, multilayer model for predicting the diurnal variations in the thermal and momentum fields in the planetary boundary layer (PBL) is proposed for incorporating into mesoscale or large-scale dynamical models. The ground temperature is given by a soil slab heated (or cooled) by net radiation and sensible heat from the atmospheric surface layer and a ground thermal reservoir. The surface heat flux can be generated by two mechanisms: 1) the convective mixing depending on the temperature difference between the ground and the screen level and 2) the mechanical mixing depending on the wind stress. Following Blackadar (1976), a prediction equation is employed for the screen-level temperature. In the PBL, the heat and momentum exchanges are computed by a Richardson number adjustment scheme. Heat and momentum exchanges occur mainly due to thermal instability under convectively unstable conditions and due to shear instability under convectively stable conditions. A case study shows good agreement between model results and observation. Additional experiments are performed to test the scheme under calm and stronger wind situations. Since no explicit diffusion coefficient is needed in the adjustment scheme, the model time step is not restricted by computational stability requirements of the diffusion term. This PBL parameterization scheme is therefore very appealing for use in numerical models that use large time steps yet have good vertical resolutions in the PBL.

1. Introduction

One of the most pronounced diurnal variations in all meteorological phenomena is the one associated with the characteristics of the planetary boundary layer (PBL). In the early morning, when the solar radiation incident on the top soil starts to increase and gradually compensate for the net radiative cooling, heat transfer from the surface takes place with ascending thermals whose potential temperature is that of the surface layer. As these thermals ascend, they mix with the air and increase the temperature of the potentially cooler air layers above. As the day goes on and the net radiation increases, the potentially cooler layers near the surface are heated up. The thermals and thus the mixing are bounded by the capping inversion layer with strong negative buoyancy. Sometimes the thermals are energetic enough to overshoot into the potentially warmer layer above the inversion with the consequent cooling there. Below this capping inversion, the potential temperature, momentum and moisture are so well mixed that the eddy fluxes are not related to the local gradients. These buoyant thermals may induce upward heat fluxes opposite to the local gradients (e.g., Priestley and Swinbank, 1947; Deardorff, 1966).

The complexity of the PBL behavior in the stable condition does not cease with the convective activities as pointed out by Businger (1973). In the mid-afternoon the entire boundary layer is in turbulent motion because there are both buoyant and shear energy productions. Since the wind shear is large near the surface, the Richardson number is always small and increases with height to some level. Sometime in the late afternoon when the incoming solar radiation at the ground cannot compensate for the infrared radiation, the surface heat flux changes to downward. A laminar layer will form relatively close to the surface and dampen the turbulence and prevent the eddy fluxes from above. Below the laminar layer, the transfer of momentum and heat will continue to the surface. As the available momentum is gradually depleted, the surface wind diminishes and a period of calm sets in. The temperature near the surface drops quickly during this period because the outgoing radiation is not balanced by downward heat flux. In the meantime, above the laminar layer where the velocity is usually sub-geostrophic in daytime, wind speed increases accelerated by the Coriolis force. As a consequence, the wind shear increases, and the Richardson number decreases and eventually reaches a value below the critical value. A turbulent burst of momentum and heat will break through the laminar layer and reach the surface. When this occurs, the wind shear will decrease and the temperature lapse rate will moderate below the laminar layer. However, as the radiative cooling continues, the entire sequence of events may repeat. These intermittent episodes of turbulent mixing in a stable boundary layer are often observed.

0021-8952/79/091205-11$06.75

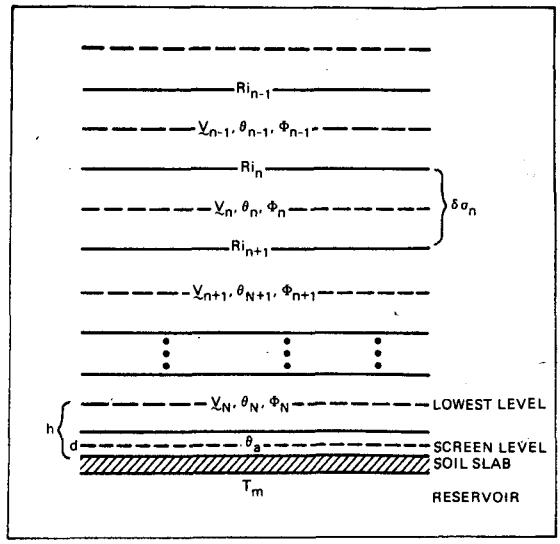

FIG. 1. The vertical structure of the model.

In general, two approaches toward modeling the phenomena of the PBL and investigating the interaction of the PBL with the large-scale flow are possible (Clarke, 1970a; Deardorff, 1972; Busch *et al.*, 1976). The first method is to relate the behavior and gross effects of the PBL to a number of external parameters. The internal structure of the PBL is assumed *a priori;* the height of the PBL is explicitly predicted (Deardorff, 1972; Tennekes, 1973). The drawback of this type of PBL model is its failure to deal with the stable boundary layer, especially at the transition from unstable conditions to stable conditions.

The second approach is to resolve the structure of the boundary layer explicitly by including several computational levels within the boundary layer. The height of the PBL can be diagnosed from PBL structure, and some form of K coefficients is used to relate various fluxes with the mean local gradients (Lumley and Panofsky, 1964). Although this assumption may be reasonably satisfied for the stable or nighttime PBL when the scale of turbulence is small, it fails in daytime mixed layers because the scale of the convection cannot be separated from the scale of mixed-layer depth. Recently, attempts have been made to develop higher order closure models (Donaldson, 1973; Lumley and Khajeh-Nouri, 1974; Wyngaard *et al.*, 1974; Zeman and Lumley, 1976). These models, while quite useful in studying the structure of turbulence in free convection, require enormous amount or computational resources. In addition, some of the closure assumptions have not been fully tested. To incorporate such complicated schemes into the already complex problem of mesoscale or large-scale dynamical systems still remains a challenging but prohibitive task.

The purpose of this paper is to propose a simple method for predicting diurnal variations in the thermal and momentum structures of the PBL, with special provisions for incorporation into either mesoscale or large-scale dynamical models. The mixing within the daytime PBL is visualized as being performed by the buoyantly driven thermals with roots near the surface. The exchange of heat takes place in layers which are thermally unstable relative to the surface. Assuming that the momentum is conserved during the mixing process, the exchange of momentum is regulated by the rate of heat exchange. The mixing in the stable nighttime PBL occurs only when the shear production of turbulent kinetic energy is strong enough. A soil slab-model of Blackadar's (1976) is utilized to yield proper surface heat flux. The net solar radiation depends on the solar zenith angle, surface albedo and atmospheric turbidity. The effect of moisture is neglected in this study pending further research on latent energy balance in the soil.

In the next section, the proposed PBL scheme will be discussed. In Section 3, some computational considerations for a better solution are explored. The result of some specific simulations will be illustrated in Section 4.

2. The PBL model

For simplicity, only one dimension is considered here; the extension to two or three dimensions is straightforward by the inclusion of the horizontal advective effects, assuming the small-scale turbulent structure of the PBL is horizontally quasi-homogeneous at each grid point. The governing equations of the model can be written as

$$\frac{\partial u}{\partial t} = f(v-v_g) + \left(\frac{\delta u}{\delta t}\right)_m, \tag{1}$$

$$\frac{\partial v}{\partial t} = -f(u-u_g) + \left(\frac{\delta v}{\delta t}\right)_m, \tag{2}$$

$$\frac{\partial \theta}{\partial t} = \left(\frac{\delta \theta}{\delta t}\right)_m, \tag{3}$$

where u, v and θ represent velocity components and potential temperature, respectively. The subscript m denotes the effect of turbulent mixing. The vertical structure of the model is shown in Fig. 1. A σ coordinate in the vertical is used to facilitate the incorporation into mesoscale or large-scale dynamical models. The time-dependent variables u, v and θ are defined at the center of each σ layer; the gradients, various fluxes and the Richardson number are defined at the interfaces between σ layers.

a. *The soil and surface layer*

The soil slab model used here is designed by Blackadar (1976) to predict the ground surface temperature T_g (symbols and their values are listed in Appendix).

This soil slab model has been tested by Deardorff (1978) and was found to be superior to other six soil models. A slightly modified version of this model also performed well in a mesoscale dynamical model (Anthes and Warner, 1978).

In this soil model, the ground temperature is predicted by

$$\frac{\partial T_g}{\partial t}=(I_s\downarrow+I_L\downarrow-I_L\uparrow)C_g^{-1}+\omega(T_m-T_g)+K_s(\theta_a-T_g). \quad (4)$$

The terms on the right represent the effects of the solar radiation and the atmospheric backscattering radiation, the longwave surface radiation, the heat exchange with deep soil, and the heat exchange with overlying atmospheric surface layer, respectively. The numerical value used for the relaxation constant ω is such that the temperature oscillation in the soil slab has appropriate time scale. Another relaxation constant K_s should have the same magnitude as ω and ought to be a function of wind speed. However, it is the product of K_s and (θ_a-T_g) which yields the heat flux and the model result is insensitive to the precise value of K_s as indicated by supplementary sensitivity tests.

The solar radiation is estimated by

$$I_s\downarrow=S\cos Z(1-A)q^{\sec Z}, \quad (5)$$

where S is the solar constant, A the surface albedo and q the atmospheric turbidity. The zenith angle Z is obtained from the local hour angle h_s, latitude ϕ and solar inclination angle δ; i.e.,

$$\cos Z=\cos h_s\cos\phi\cos\delta+\sin\phi\sin\delta. \quad (6)$$

For longwave radiation, we ignore the effect of water vapor and use a simple Brunt's equation (Seller, 1965) to estimate the net infrared radiation, i.e.,

$$I_L\downarrow-I_L\uparrow=-\epsilon(1-0.61)\beta T_g^4. \quad (7)$$

As indicated by Blackadar (1976), the heat capacity C_g in (4) should be

$$C_g=\left(\frac{\lambda C_s}{2\omega}\right)^{\frac{1}{2}}, \quad (8)$$

where λ and C_s are the soil thermal conductivity and the soil heat capacity per unit volume, respectively. Typical numerical values of various soil constants used here can be found in Geiger (1966).

The surface layer is defined as the layer that regulates the passage of heat from the ground to the atmosphere. It has a depth d, about twice that of the screen level. Assuming that there is no diabatic heat source (such as condensation) in the surface layer, the balance of heat requires

$$\frac{\partial\theta_a}{\partial t}=\frac{C_g}{\rho C_p d}K_s(T_g-\theta_a)-\frac{H_0}{\rho C_p d}, \quad (9)$$

where the density variation over the depth d is neglected. The terms on the right side of (9) represent the heat exchange between the surface layer and the ground and the sensible heat flux from the surface layer into the mixed layer. The total surface heat flux H_0 is the sum of the convective heat flux H_c and the mechanical heat flux H_m.

For convective conditions ($\theta_a>\theta_N$), Priestley (1956) pointed out that the convective surface heat flux H_c is proportional to the $\frac{3}{2}$ power of the vertical temperature difference. Mathematically, given that

$$B=\left(\frac{2g}{27\theta_a}\right)^{\frac{1}{2}}\frac{h^*}{d}(d^{-\frac{1}{3}}-2h^{-\frac{1}{3}})^{-\frac{1}{2}}, \quad (10)$$

we have

$$H_c=\rho C_p Bd(\theta_a-\theta_N)^{\frac{3}{2}}, \quad (11)$$

where θ_N is the potential temperature of the lowest layer at height h, and h^* is the Priestley constant, taken to be unity. Heat flux can also be generated by wind shear acting on the gradient of potential temperature near the surface, which is the only mechanism to cause heat exchange in nonconvective situations ($\theta_a\leqslant\theta_N$). The heat flux generated by shear and surface wind stress are evaluated by the nondimensional gradient equations based on Monin-Obukhov simularity theory:

$$H_m=-\rho C_p u_*\theta_*. \quad (12)$$

Here u_* and θ_* are frictional velocity and frictional temperature, defined by

$$\frac{|\mathbf{V}_N|}{u_*}=\frac{1}{\kappa}\left[\ln\left(\frac{h}{z_0}\right)-\psi_m\left(\frac{h}{L}\right)\right], \quad (13)$$

$$\frac{\theta_N-\theta_a}{\theta_*}=0.74\left[\ln\left(\frac{h}{z_a}\right)-\psi_h\left(\frac{h}{L}\right)\right], \quad (14)$$

where ψ_m and ψ_h are universal stability functions (Businger, 1973). The Monin-Obukhov stability parameter h/L is defined as

$$\frac{h}{L}=-\frac{\kappa ghH_m}{\rho C_p\theta_a u_*^3}. \quad (15)$$

For a strongly buoyant surface layer, $(\theta_a-\theta_N)$ is large, u_* is small, and the magnitude of H_c is much larger than that of H_m; for a strongly sheared surface layer, $(\theta_a-\theta_N)$ is small, u_* is large, and the magnitude of H_c is much smaller than H_m. Therefore, H_0 $(=H_m+H_c)$ yields a reasonable surface heat flux, although H_m includes some influence of convection through its dependence on ψ_h. The results discussed in Section 4 confirms this by illustrating that the surface heat fluxes differ only slightly for calm and windy conditions (Fig. 6).

Once u_* and H_0 are determined from the surface layer, the effects due to mixing are realized in the lowest layer

of the model by

$$\left(\frac{\partial u_N}{\partial t}\right)_m = -\frac{u_*^2}{h}\frac{u_N}{|\mathbf{V}_N|}, \tag{16}$$

$$\left(\frac{\partial v_N}{\partial t}\right)_m = -\frac{u_*^2}{h}\frac{v_N}{|\mathbf{V}_N|}, \tag{17}$$

$$\left(\frac{\partial \theta_N}{\partial t}\right)_m = \frac{\theta_N}{T_N}\frac{H_0}{\rho C_p h}. \tag{18}$$

To distribute the momentum and the heating (cooling) to other layers above layer N, we now propose an adjustment scheme.

b. Richardson number adjustment scheme below the "inversion"

The atmosphere is usually well mixed below the inversion. Under convective conditions, the mixing is dominated by the turbulent eddies of various size and strength originating from the surface. Under stable conditions, sheer-induced mixing is the dominant mechanism. When a stability criterion between two layers has reached a certain critical value—either due to buoyance or wind shear—the air in the two layers is mixed and adjusted to a more stable state. We propose to use the gradient Richardson number, defined by

$$\mathrm{Ri} = -\frac{g}{\theta}\frac{\partial\theta}{\partial z}\Big/\left[\left(\frac{\partial u}{\partial z}\right)^2+\left(\frac{\partial v}{\partial z}\right)^2\right], \tag{19}$$

as the criterion for mixing since it has been studied extensively in both theoretical and experimental studies of turbulence. The mixing can then be induced by static instability in convective and near neutral conditions, and by wind shear in stable condition.

Different values of a critical Richardson number ($\mathrm{Ri_{cr}}$) for the onset or termination of turbulence have been found by various investigators. There are two different approaches to this problem, the first of which is relevant to the transition from turbulent to laminar flow. Because the production terms contain the fluxes, the flux Richardson number is the relevant parameter. Assuming that the eddy transfer coefficients for heat and momentum are equal and that the viscous dissipation is absent, Richardson (1920) argued that $\mathrm{Ri_{cr}}=1$. This means that shear production of turbulent kinetic energy is balanced by the negative buoyant production. Since viscous dissipation is an energy sink not to be neglected and the eddy transfer coefficients for heat and momentum are not equal in reality, $\mathrm{Ri_{cr}}$ should be smaller than what Richardson suggested. Several investigations have been made to refine Richardson's analysis (e.g., Ellison, 1957; Townsend, 1958). These theories all yield values of $\mathrm{Ri_{cr}}<1$. A recent study by Arya (1972) suggested a value in the neighborhood of 0.2. This value is supported by the analysis of Businger *et al.* (1971) of the 1968 Kansas Experiment (Haugen *et al.*, 1971).

In the second approach, the transition from laminar to turbulent flow is considered. This approach leads to the critical Richardson number since the gradients are well defined. A value of $\frac{1}{4}$ for $\mathrm{Ri_{cr}}$ was reached by Taylor (1931) and later by Miles (1961) with refinements. Using the technique of exchange of air parcels, Ludlam (1967) gave $\mathrm{Ri_{cr}}=0.25$. Businger (1969) later extended Ludlam's analysis and showed that $\mathrm{Ri_{cr}}$ varies from $\frac{1}{4}\sim 1$. Experimental analyses by Woods (1969) and Hines (1971) supported Businger's finding.

Careful experimental work is needed to determine precisely a value for $\mathrm{Ri_{cr}}$. Here, we let $\mathrm{Ri_{cr}}=\frac{1}{4}$, which seems to be in best agreement with various studies.

Let θ_n and θ_{n+1} denote the potential temperatures of two adjacent layers (Fig. 1) between which $\mathrm{Ri}<\frac{1}{4}$, and let θ_n' and θ_{n+1}' denote the potential temperatures after the adjustment in these two layers. It is suggested that a lapse rate Γ_c is established after the adjustment so that

$$\theta_n'-\theta_{n+1}'=\frac{\Gamma_c}{g}(\Phi_n-\Phi_{n+1}). \tag{20}$$

Deardorff (1966) suggested that a value of 7×10^{-4} K m^{-1} for Γ_c to account for the countergradient heat flux. In addition, a positive Γ_c decreases the number of adjustments needed when the stability of all layers below the inversion are checked.

Based on the concept that the potential temperature is conserved during adiabatic mixing, and by using (20), we have

$$\theta_n'=\frac{\theta_n\delta\sigma_n+\theta_{n+1}\delta\sigma_{n+1}+\Gamma_c(\Phi_n-\Phi_{n+1})g^{-1}\delta\sigma_{n+1}}{\delta\sigma_n+\delta\sigma_{n+1}}. \tag{21}$$

From the above, the proportion α of mass in layer $n+1$ mixed into layer n in order for θ_n to adjust to θ_n' can be obtained, i.e.,

$$\alpha=\frac{\theta_n'-\theta_n}{\theta_{n+1}-\theta_n}. \tag{22}$$

The adjustment of momentum is obtained by mixing the same α portion of mass of layer $n+1$ into layer n,

$$\mathbf{V}_n'=(1-\alpha)\mathbf{V}_n+\alpha\mathbf{V}_{n+1}, \tag{23}$$

and by conservation of momentum,

$$\mathbf{V}_{n+1}=\frac{(\mathbf{V}_n-\mathbf{V}_n')\delta\sigma_n+\mathbf{V}_{n+1}\delta\sigma_{n+1}}{\delta\sigma_{n+1}}. \tag{24}$$

After the adjustment is carried out for layers n and $n+1$ we again compare the Richardson number between layers $n-1$ and n. This procedure is carried out until the layer where $\mathrm{Ri}>\frac{1}{4}$ is reached. For strongly convec-

tive conditions in which the scale of the eddy is equivalent to the depth of the boundary layer, the above adjustment should be repreated several times, so that the heating at the surface layer can be mixed throughout the boundary layer.

Note that $(\delta u/\delta t)_m$, $(\delta v/\delta t)_m$ and $(\delta\theta/\delta t)_m$ in Eqs. (1)–(3) are evaluated implicitly for all layers by the adjustment in Eqs. (20)–(24); therefore, there is no explicit expressions for them. The corresponding mixing for moisture or pollutant in the PBL follows the same form as (23) and (24).

3. Computational considerations

In each time step, the computation cycle starts with the evaluation of the net radiation transmitted to the ground layer at the local time with Eqs. (6) and (7). Then, the ground temperature T_g is forecast by (4). It is followed by computing the surface fluxes of heat and momentum with Eqs. (10)–(15). The next step is to forecast the surface temperature θ_a and store it for the next time step.

The governing equations (1)–(3) are integrated foreward in time. The inviscid terms in the governing equations are estimated for each grid point; however, the viscous terms are computed only for the lowest layer using (16)–(18). Thus, tentative values of u, v, and θ are obtained for each grid point.

The Richardson number adjustment scheme begins with a computation of the Richardson number for every two adjacent layers based on the tentative values of u, v and θ. Starting from the lowest two layers, the adjustments [Eqs. (20)–(24)] are carried out for every two adjacent layers if the stability criterion is exceeded. The adjustments proceed until all the layers are checked. Since an adjustment between layers n and $n+1$ would alter the stability between layers n and $n-1$, the new Richardson numbers are computed once more and necessary adjustments are again carried out. This process is repeated several times until a desired stability is reached. In doing so, a heating (or cooling) in the surface layer could affect the higher layers unless prevented from doing so by a layer of strong stability or a capping inversion. For the case study discussed below, the number of repetitions is limited to five.

In some PBL models in which K coefficients are used, the time steps δt are sometimes restricted by the requirements of computational stability, i.e.,

$$\delta t < \tfrac{1}{4}\frac{K_{\max}}{(\Delta z)^2}, \tag{25}$$

where $K_{\max}$ is the maximum value of K coefficient and Δz the height increment. For strong heating conditions when the value of $K_{\max}$ becomes very large, the time step can be restricted to only several seconds (Busch *et al.*, 1976, Blackadar, 1976). Here a constant time step of 300 s is used. The adjustment scheme used here is always computationally stable.

In predicting the surface potential temperature θ_a, a computational instability is encountered. For example, a positive anomaly of θ_a would give a positive anomaly of H_0 through (11), which in turn would result in a negative anomaly of θ_a through (9). This instability is avoided by taking a 30 s time step when computing θ_a and T_g.

Parcels of heated air rising from the surface layer under convective conditions usually possess enough kinetic energy to overcome friction so that they sometimes penetrate into the overlying stably stratified layer before being overcome by the negative buoyancy. The mixing of the overshooting parcels with the environment produces commonly observed cooling in the capping stable layer. The effect of overshooting is simulated in the present model by artificial mixing of a small amount of air across the inversion. The amoung of mixing is determined by setting

$$\alpha = a\frac{\alpha\sigma_{n+1}}{\delta\sigma_n}, \quad \text{if} \quad H_0 > 0, \tag{26}$$

when n is the level above which $\mathrm{Ri} > \frac{1}{4}$ and a is set to 0.1.

In the case study discussed in the next section, a uniform vertical resolution of $\delta\sigma = 0.01$ in the model has been used in order to show the detailed PBL structure. Experiments with a coarser grid and a stretched grid yield results similar to those obtained with the uniform grid. The optimal grid structure for use in a dynamic model should be chosen based on the specific needs and restructions of the individual mesoscale or large-scale model.

4. A case study

The observational data of the Great Plains Experiment on day 9 of August 1953 are chosen for use in the model. Suitable values of constants are determined for O'Neill, Nebraska, and are listed in the Appendix. On the day selected, it is evident in the observational data that there was warm advection with a heating rate of ~ 0.5°C h^{-1} above the 700 m level during the daytime. This effect is not taken into account here. Since the pressure-gradient force was not determined precisely, no verification of wind speed will be attempted. Instead, vertically uniform geostrophic winds speeds of 0 (Case 1), 5 (Case 2) and 10 m s^{-1} (Case 3) are used to test the model under calm, weakly windy and moderately windy situations. Model starting time is 0435 LST. The quasi-steady initial wind fields for Cases 2 and 3 are generated by the same procedure used for the initial condition in Busch *et al.* (1976). Due to the strong mixing initiated in early morning, the model results are insensitive to the initial wind field. However, the model results are sensitive to the

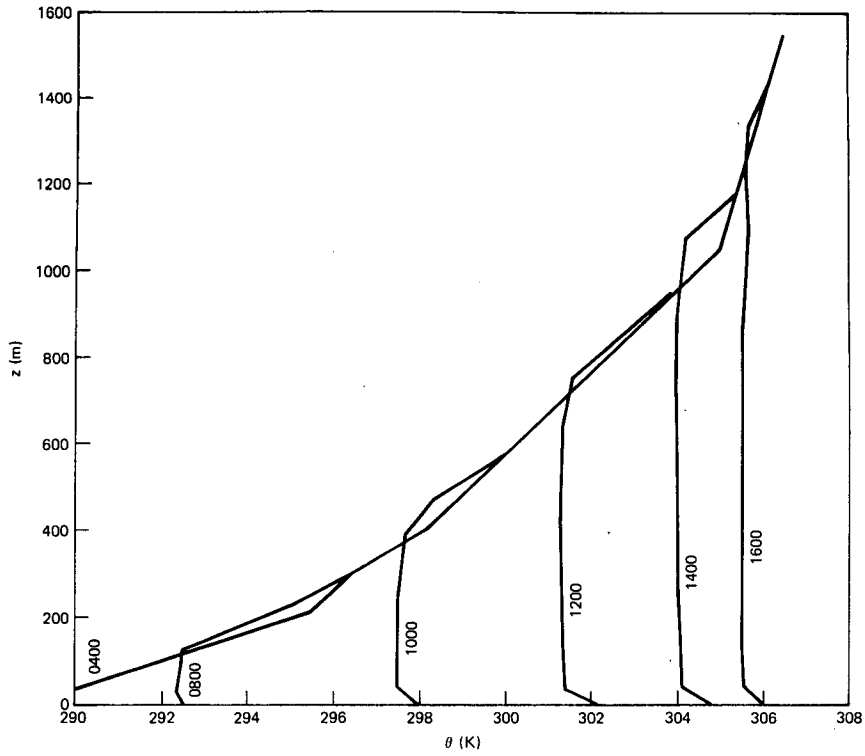

FIG. 2. The observed initial potential temperature and the predicted potential temperature in the PBL. The labels denote local times in hours.

initial temperature field. The initial temperature profile shows a deep inversion extending from the surface to about 1000 m (Fig. 2).

a. The soil and screen level temperature

The soil temperatures for the three cases are shown in Fig. 3. The variation of the soil temperature closely follows the net infrared radiation with a lag of ~1 h. The daytime soil temperatures for three cases are very similar. The soil temperature of Case 1 ($u_g=0$ m s^{-1}) is about 1°C higher at its peak than the soil temperature of Case 3 ($u_g=10$ m s^{-1}). This is because the wind shear in Case 3 induces stronger upward heat flux in the convective situation. In the nighttime, however, the soil temperature of Case 1 is lower than that of Cases 2 and 3. The difference between Cases 1 and 3 increases to more than 6°C after midnight. This is due to the fact that the downward heat flux from layers above is almost completely cutoff in the calm situation.

The diurnal variations of the screen-level (1 m) temperature for three cases are shown in Fig. 4. The highest temperature at the screen level occurs at approximately 1400–1600 LT as often observed. Notice that the screen-level temperature decreases quickly after 1900 LT as the ground temperature becomes lower than the screen-level temperature. The relation-

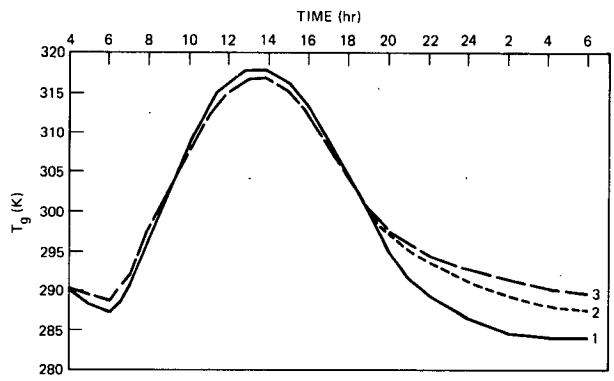

FIG. 3. The predicted diurnal variations of soil temperature for Cases 1 ($u_g=0$ m s^{-1}), 2 ($u_g=5$ m s^{-1}), 3 ($u_g=10$ m s^{-1}).

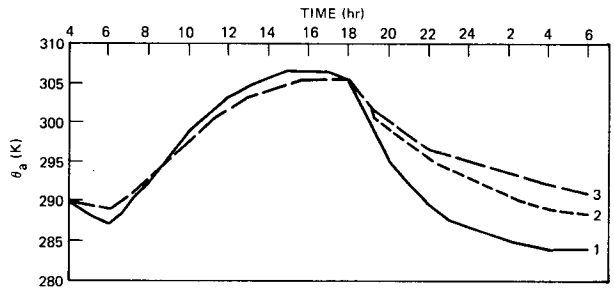

FIG. 4. As in Fig. 3 except for the screen level temperature.

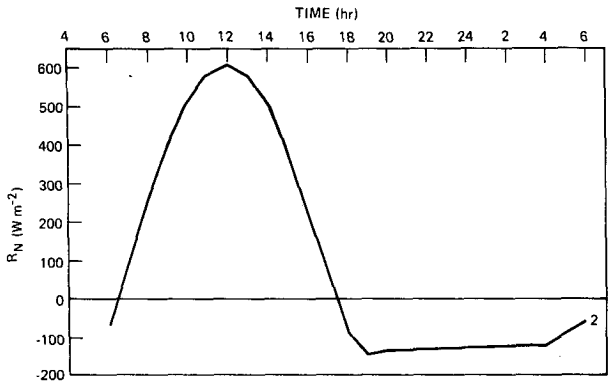

FIG. 5. The net radiation flux for Case 2.

ship between the three cases is similar to that of the ground temperature, i.e., the screen-level temperature of Case 3 ($u_g = 10$ m s^{-1}) is ~ 1°C cooler in daytime and 6–7°C warmer in nighttime than that of Case 1 (calm). Again, wind shear is needed for turbulent heat transfer from higher levels in non-convective conditions.

b. The net radiation and the surface sensible heat flux

Fig. 5 shows the net radiation flux R_N for Case 2. The net radiation flux for Case 1 and 3 is similar except that it is slightly stronger for Case 3 and slightly weaker for Case 1 in nighttime due to differences in ground temperature. The net radiation flux reaches its peak at 1200 LT. However, the net radiation is slightly asymmetrical about noon because higher ground temperature in the afternoon causes higher outgoing infrared radiation.

Since the surface sensible heat flux (H_0) is proportional to the difference between the screen-level temperature and the air temperature above, it has a phase lag of ~ 30 min with respect to the net radiation (see Fig. 6). As governed by the ground and screen level temperatures, the surface sensible heat flux of

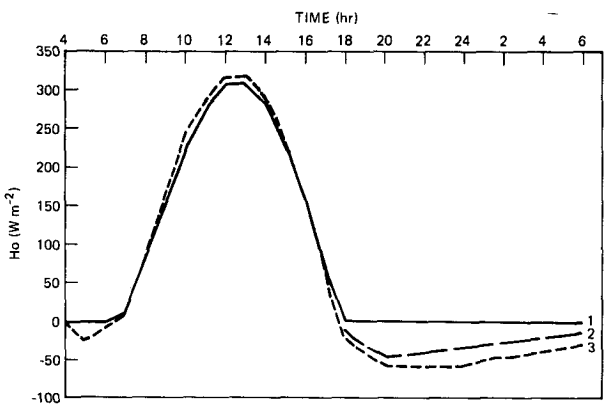

FIG. 6. The surface heat fluxes, including the convective type and the mechanical type, for Cases 1 ($u_g = 0$ m s^{-1}), 2 ($u_g = 5$ m s^{-1}), and 3 ($u_g = 10$ m s^{-1}).

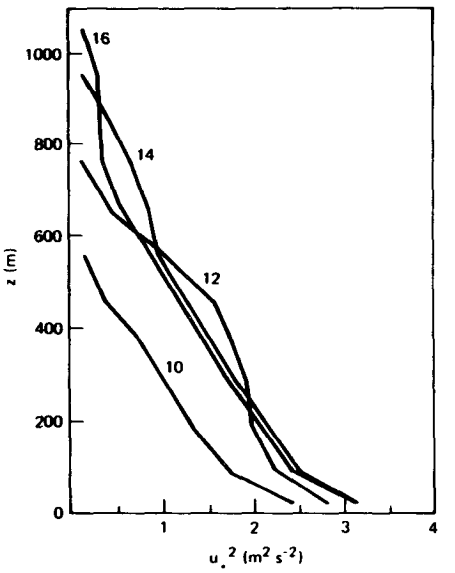

FIG. 7. The vertical profiles of the stress (u_*^2) in convective condition for Case 3 ($u_g = 10$ m s^{-1}). The labels denote local times in hours.

Case 3 is stronger in the upward direction in the daytime and stronger in the downward direction in the nighttime than cases of weaker winds. The slightly stronger upward heat flux in Case 3 indicates an enhancement of heat transfer due to wind shear. The stronger downward heat flux in Case 3 is caused by the stronger wind shear in the nighttime surface layer.

c. Temperature structure of the convective boundary layer

Since the upward heat fluxes in daytime for three cases are similar, and the sensible heat is conserved in the model, the thermal structures in the daytime convective boundary layer for three cases are similar. Fig. 2 shows the vertical temperature profiles at different times for Case 2.

After 0600 LT, the lower part of the PBL, especially the surface layer, becomes superadiabatic, and supports an upward heat flux at the surface. Above this superadiabatic layer, the lapse rate is slightly stable throughout the PBL, as noted by Clarke (1970b) in the study of the Wangara experiment data. The weakly stable lapse rate here is a consequence of the overadjustment of potential temperature to account for the countergradient upward heat flux.

The overshooting of the PBL and sharpening of the capping inversion, commonly observed and described in detail by Deardorff (1974), Busch *et al.* (1976) and Zeman and Tennekes (1977), are produced by the mixing across the inversion. As indicated by the study of Zeman and Tennekes (1977), the proportionality constant a in (26) should depend on the local mechanical production and dissipation rates. However, the model

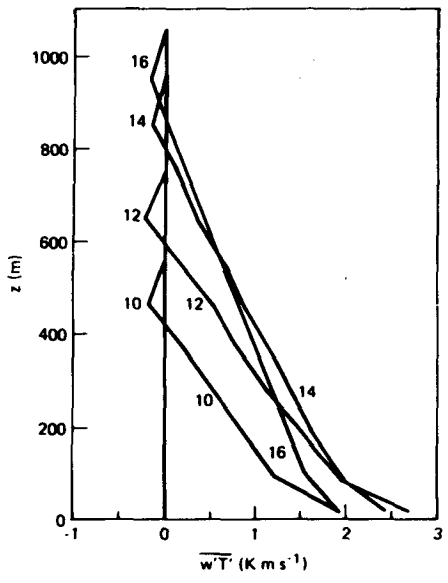

FIG. 8. The vertical profiles of the heat flux ($\overline{w'T'}$) in convective conditions for Case 3 ($u_g=10$ m s^{-1}). The labels denote local times in hours.

seems to produce a reasonably good prediction of temperature for this particular case for $a=0.1$.

Despite a set of constants selected *a priori* for the model, the predicted temperature of the PBL agrees well with the observation within 1–2°C (Lettau and Davidson, 1957).

d. The momentum and heat fluxes in the convective PBL

The momentum and heat fluxes, though not explicitly computed in our model, can be diagnosed from the rates of change and the boundary values.

The vertical profiles of momentum flux of Case 3 in the convective PBL are shown in Fig. 7. The profiles in general decrease linearly with height except that the rate of decrease is larger below 100 m. The vertical profiles of momentum flux in Case 2 are similar in character but smaller in magnitude.

The vertical profiles of heat flux of Case 3 in the convective PBL are shown in Fig. 8. Similar to the momentum fluxes, the heat flux in the convective PBL varies linearly with height in most parts of the PBL except for a first-order discontinuity at 100 m. There is a downward heat flux at the top of the PBL. Lilly (1968) and Willis and Deardorff (1974) showed that the magnitude of this downward heat flux falls in the range 13–25% of H_0 for different strengths of the inversion. Its value can reach as much as 50% of H_0 (Carson, 1973; Tennekes and Van Ulden, 1974). As derived by Zeman and Tennekes (1977), the ratio of the downward flux to the surface heat flux is a function of the PBL height, the convective velocity scale and the strength of the inversion. Improvement can be made in formulating (26) based upon these studies, but it will inevitably complicate the present scheme.

In general, the vertical profiles of the momentum and heat fluxes as shown in Figs. 7 and 8 exhibit similar characteristics with other more complex models (e.g., Deardorff, 1974; Wyngaard and Coté, 1974; Shir, 1973; Stull, 1973; Busch *et al.*, 1976) and observations.

e. Formation of the nocturnal low-level jet

As the radiational cooling produces a stable layer near the surface, the heat transfer and therefore the momentum transfer between the surface layer and air layers above are effectively suppressed. The commonly sub-geostrophic flow in the daytime PBL will be accelerated by the Coriolis force at a rate proportional to the magnitude of the ageostrophic wind vector (Blackadar, 1957). The direction of the acceleration is at a right (clockwise in Northern Hemisphere) angle to that vector.

The hodograph of the ageostrophic wind vectors at levels of 1000 and 1200 m in Fig. 9 shows the increasing acceleration after sunset. Notice that the air flow at 1000 m is not affected by the mixing until midday when the inversion is rising to a level higher than 1000 m (Fig. 2). By comparison, it is clear that the inertial acceleration is larger at 1000 m where the wind has been more sub-geostrophic in daytime. The vertical wind profiles after sunset (Fig. 10) illustrate the formation of the nocturnal jet at low levels. At 0000 LT, the speed of

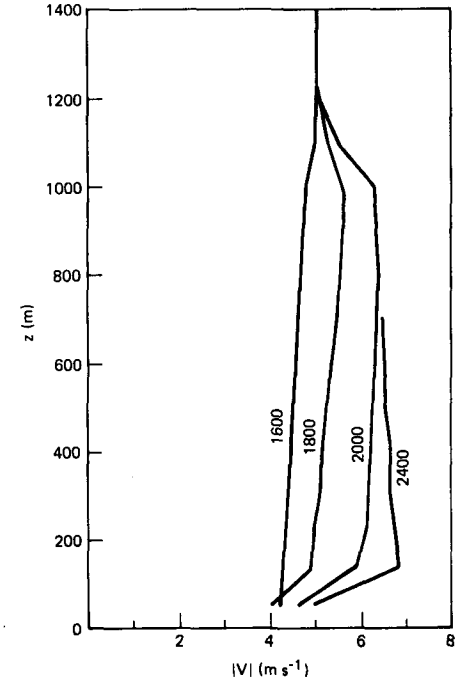

FIG. 9. The hodograph of the ageostrophic components ($u-u_g$, $v-v_g$) of the PBL winds at 1000 and 1200 m levels.

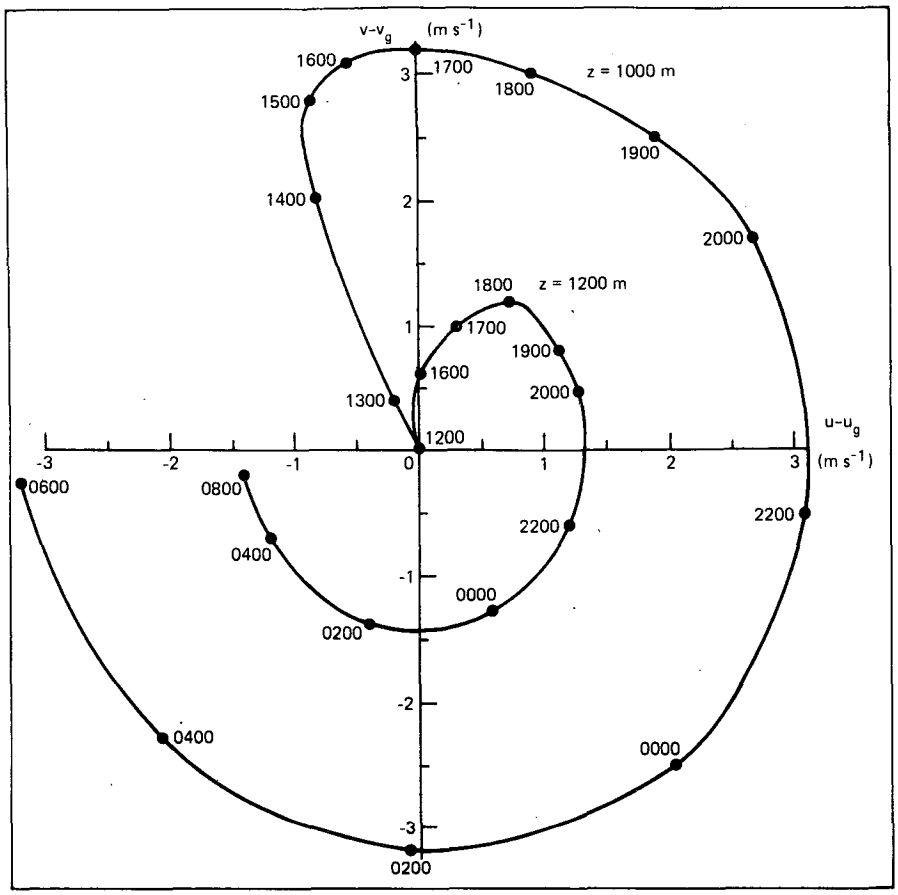

FIG. 10. The vertical profiles of the PBL wind speeds at indicated local times showing the development of the nocturnal low-level jet.

the jet is 40% greater than the geostrophic wind speed. The vertical wind shear near the surface is very strong at this time and overturnings occur frequently.

f. Episodes of overturning in the stable PBL

It is well known that the surface temperature drops more rapidly on a calm night than it does on a windy night, since no downward turbulent heat transfer occurs to compensate for the radiative cooling in lieu of wind shear. The heat transfer in this situation is mainly through molecular diffusion, which is several orders of magnitude smaller. On a windy night the turbulent transfers are generated by wind shear and occur intermittently (Businger, 1973; Blackadar, 1976).

The time interval between episodes depends on several factors, including the magnitudes of the geostrophic wind, Coriolis parameter and the surface roughness. As is commonly shown on aneometer and thermometer strip charts, both the velocity and temperature oscillate suddenly at the early stage of one episode indicating that a turbulent burst breaks through the laminar layer. These initial oscillations are followed by the lingering oscillations at lower frequencies with indication of some gravity wave effects. The evolution of such overturning is described in Section 1.

Fig. 11 shows the potential temperature change for every 5 min, $\theta_a(t)-\theta_a(t+5)$, in Case 3. Positive values mean a cooling trend, negative values, warming. As shown by the nighttime surface temperature, there are episodes of sudden warming superimposed on continuous radiative cooling. These episodes of sudden warming are caused by the overturning as the low-level wind shear increases and the local Richardson number exceeds its critical value. The temporal variations of the surface wind components for the same time period show that the wind increases correspondingly at times of sudden warming. After the occurrence of each period, the temperature lapse rate and the wind shear near the surface moderate. However, as the surface cools continuously due to net radiation, stability increases and vertical mixing is cut off again. During this relatively calm period, the momentum immediately above the surface is continuously decreased by friction and the wind above is continuously turned by the Coriolis force. When the wind shear is large enough to cause the Richardson number to become less than the

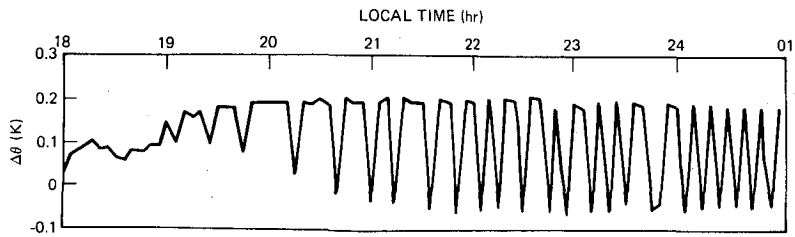

FIG. 11. The change of screen-level potential temperature over a time interval of 5 min for Case 3.

critical value, an episode of overturning again occurs. These episodes occur in a time interval of 20–30 min before 2200 LT when the cooling rate is strong. After this time, since the cooling rate decreases (see Fig. 3) and the nocturnal low-level jet forms and thus increases the low-level wind shear, the adjustments occur more frequently. There are no such episodes in Case 1 and less frequent occurrence of episodes in Case 2.

Along with the episodes of turbulent overturning, heat is transferred downward from above the surface layer. The temperature for Case 3 shows the nocturnal inversion grows to more than 500 m in this case. For a weaker wind, the inversion shows much less growth and much cooler surface temperature. For the calm situation, the temperature of the PBL is not modified except that the surface temperature is 7–8°C cooler that that in Case 3 (see Fig. 4).

5. Summary

An efficient PBL parameterization scheme is proposed. A soil slab model of Blackadar (1976) is used to give the soil and surface temperatures. The surface heat flux is calculated from both convective and mechanical mixing. The heat and momentum exchanges in the PBL are computed by a Richardson number adjustment scheme. These exchanges can occur from either thermal stability or shear instability. Since no explicit diffusion coefficient is needed, the model time step is not restricted by the computational stability requirement associated with the strong mixing. The results of a 24 h forecase agree well with the observation.

Although the higher order closure schemes have given considerable insight into the turbulent flow of the boundary layer, the simple, efficient scheme proposed here remains as a ecomonic alternative when it is necessary to describe the PBL structure in some detail in a mesoscale or large-scale dynamical model. The results discussed are simulations with a 5 min time step. One 24 h run of such simulations requires one-fifth of the running time required by the model of Busch *et al.* (1976) for similar initial conditions, external forcing and gridwork. Results from experiments with a 10 min time step indicate no appreciable deviation from those with 5 min time step. A time step of 5–10 min is comparable to those of the fine-mesh grid (4–5°) versions of the global circulation models and some mesoscale models using implicit integration schemes. The time steps of such models, even when very fine vertical resolution is desired, need not to be reduced if the PBL parameterization discussed here is utilized.

One important aspect of the earth–atmosphere interactions that has not been considered here is the effect of the ground wetness which must be included if the exchange of latent energy between the soil and atmosphere is to be realistically treated. Attempts are being undertaken to investigate the effect of the ground wetness to the characteristics of the PBL.

Acknowledgments. The influence of Professor Alfred K. Blackadar on the modeling of PBL is gratefully acknowledged. Thanks are due to reviewers whose comments have improved the clarity of the manuscript. The research was started when the author was a National Research Council postdoctoral research associate at Goddard Space Flight Center, National Aeronautical and Space Administration. The later portion of the work was supported by Naval Environmental Prediction Research Facility Block Fund through NRL Contract N00173-78-C-421. Mrs. Jane Polson and Mrs. Margaret Steinert typed the manuscript.

APPENDIX

List of Symbols[1]

A	albedo (0.2)
C_g	heat capacity of soil slab ($\rho C_p \times 80$ m)
c_s	soil heat capacity per unit volume
d	twice the depth of the screen level (2 m)
H_c	convective surface heat flux
H_m	mechanical surface heat flux
H_0	H_m+H_c
h	half-depth of the lowest model layer ($\sim$40 m)
h^*	Priestley constant (1)
h_s	local hour angle of the sun
$I_L\uparrow$	outgoing longwave radiation from the surface
$I_L\downarrow$	atmospheric backscattering longwave radiation
$I_s\downarrow$	incident solar radiation
K_s	time scale for heat conduction of air (3×10^{-4} s^{-1})
q	atmospheric turbidity (0.8)
R_n	$I_s\downarrow+I_L\downarrow-I_L\uparrow$
S	solar constant (1395 W m^{-2})

[1] The values shown for the constants have been determined from day 9 (August 1953) of the Great Plains Experiment (Lettau and Davidson, 1957).

T_m deep soil temperature (298 K)
T_n air temperature at nth layer
T_g soil slab temperature
u velocity component in the x direction
u_g geostrophic wind component in the x direction
u_* frictional velocity
$\mathbf{V}$ horizontal wind vector
v velocity component in the y direction
v_g geostrophic wind component in the y direction
Z solar zenith angle
z_a height of screen level (1 m)
z_0 surface roughness height (0.1 m)
β Stefan-Boltzman constant (5.677×10^{-8} W m^{-2} K^{-4})
δ solar inclination angle (16°)
$\delta\sigma_n$ the thickness of the nth layer
ϵ soil emissivity (0.8)
θ_a potential temperature at screen level
θ_n potential temperature at the nth layer
θ_* frictional potential temperature
λ soil thermal conductivity
Φ geopotential
ϕ latitude (42°N)
$\Psi_{m,h}$ universal stability functions
ω time scale for heat conduction in soil (7×10^{-5} s^{-1})

REFERENCES

Anthes, R. A., and T. T. Warner, 1978: Development of hydrodynamic models for air pollution and other mesometerological studies. *Mon. Wea. Rev.*, **106**, 1045–1078.

Arya, S. P. S., 1972: The condition for the maintenance of turbulence in stratified flows. *Quart. J. Roy. Meteor. Soc.*, **98**, 264–273.

Blackadar, A. K. 1957: Boundary layer wind maxima and their significance for the growth of nocturnal inversions. *Bull. Amer. Meteor. Soc.*, **38**, 283–290.

——, 1976: Modeling the nocturnal boundary layer. *Preprints Third Symp. Atmospheric Turbulence, Diffusion and Air Quality*, Raleigh, Amer. Meteor. Soc., 46–49.

Busch, N. E., S. W. Chang and R. A. Anthes, 1976: A multi-level model of the planetary boundary layer suitable for use with mesoscale dynamics models. *J. Appl. Meteor.*, **15**, 909–919.

Businger, J. A., 1969: Note on the critical Richardson number (5). *Quart. J. Roy. Meteor. Soc.*, **95**, 653–654.

——, 1973: *Workshop on Micrometeorology*, D. A. Haugen, Ed. Amer. Meteor. Soc., 67–98.

——, J. C. Wyngaard, Y. Izumi and E. F. Bradley, 1971: Flux profile relationships in the atmospheric surface layer. *J. Atmos. Sci.*, **28**, 181–189.

Carson, D. J., 1973: The development of a dry, inversion capped convectively unstable boundary layer. *Quart. J. Roy. Meteor. Soc.*, **99**, 450–467.

Clarke, R. H. 1970a: Recommended methods for the treatment of the boundary layer in numerical models of the atmosphere. *Aust. Meteor. Mag.*, **18**, 51–73.

——, 1970b: Observational studies in the atmospheric boundary layer. *Quart. J. Roy. Meteor. Soc.*, **96**, 91–114.

Deardorff, J. W. 1966: The countergradient heat flux in the lower atmosphere and in the laboratory. *J. Atmos. Sci.*, **23**, 503–506.

——, 1972: Parameterization of the planetary boundary layer for use in general circulation models. *Mon. Wea. Rev.*, **100**, 93–106.

——, 1974: Three-dimensional numerical study of turbulence in an entraining mixed layer. *Bound. Layer Meteor.*, **7**, 199–226.

——, 1978: Efficient prediction of ground surface temperature and moisture with inclusion of a layer of vegetation. *J. Geophys. Res.*, **83**, 1889–1904.

Donaldson, C. duP. 1973: *Workshop on Micrometeorology*, D. A. Haugen, Ed. Amer. Meteor. Soc., 217–268.

Ellison, T. H., 1957: Turbulent transport of heat and momentum from an infinite rough plate. *J. Fluid Mech.*, **2**, 456–466.

Geiger, R., 1966: *The Climate Near the Ground*. Harvard University Press., 611. pp.

Haugen, D. A., J. C. Kaimal and E. F. Bradley, 1971: An experimental study of Reynolds stress and heat flux in the atmospheric surface layer. *Quart. J. Roy. Meteor. Soc.*, **97**, 168–180.

Hines, C. O., 1971: Generalizations of the Richardson criterion for the onset of atmospheric turbulence. *Quart. J. Roy. Meteor. Soc.*, **97**, 429–439.

Lettau, H. H., and B. Davidson, 1957: *Exploring the Atmosphere's First Mile*, Vol. 2. Pergamon Press, 201 pp.

Lilly, D. K., 1968: Models of cloud-topped mixed layers under a strong inversion. *Quart. J. Roy. Meteor. Soc.*, **94**, 292–309.

Ludlam, F. H., 1967: Characteristics of billow clouds and their relation to clear-air turbulence. *Quart. J. Roy. Meteor. Soc.*, **93**, 419–435.

Lumely, J. L., and B. Khajeh-Nouri, 1974: Computational modeling of turbulent transport. *Advances in Geophysics*, Vol. 18A, Academic Press, 169–192.

——, and H. A. Panofsky, 1964: *The Structure of Atmospheric Turbulence*. Wiley, 239 pp.

Miles, J. W., 1961: On the stability of heterogeneous shear flows. *J. Fluid Mech.*, **11**, 284–290.

Priestly, C. H. B., 1956: Convection from the earth's surface. *Proc. Roy. Soc. London*, **A238**, 287–304.

——, and W. C. Swinbank, 1947: Vertical transport of heat by turbulence in the atmosphere. *Proc. Roy. Soc. London*, **A189**, 543–561.

Richardson, L. F., 1920: The supply of energy from and to atmospheric eddies. *Proc. Roy. Soc. London*, **A97**, 354–373.

Seller, W. D., 1965: *Physical Climatology*. University of Chicago Press, 53–54.

Shir, C. C., 1973: A preliminary numerical study of atmospheric turbulent flows in the idealized planetary boundary layer. *J. Atmos. Sci.*, **30**, 1322–1339.

Stull, R. B., 1973: Inversion rise model based on penetrative convection. *J. Atmos. Sci.*, **30**, 1092–1099.

Taylor, G. I., 1931: Effect of variation in density on the stability of superposed streams of fluids. *Proc. Roy. Soc. London*, **A132**, 499–523.

Tennekes, H., 1973: A model for the dynamics of their inversion above a convective boundary layer. *J. Atmos. Sci.*, **30**, 558–569.

——, and A. P. van Ulden, 1974: Short term forecasts of temperature and mixing height on sunny days. *Preprints Symp. Atmospheric Diffusion and Air Pollution*, Santa Barbara, Amer. Meteor. Soc., 35–40.

Townsend, A. A. 1958: Turbulence flow in a stably stratified atmosphere. *J. Fluid Mech.*, **3**, 361–372.

Willis, G. E., and J. W. Deardorff, 1974: A laboratory model of the unstable planetary boundary layer. *J. Atmos. Sci.*, **31**, 1297–1307.

Woods, J. D., 1969: On Richardson's number as a criterion for laminar-turbulence-laminar transition in the ocean and the atmosphere. *Radio Sci.*, **4**, 1289–1298.

Wyngaard, J. C., and O. R. Coté, 1975: The evolution of the convective planetary boundary layer—A higher-order-closure model study. *Bound.-Layer Meteor.*, **7**, 289–308.

——, ——, and K. S. Rao, 1974: Modeling the atmospheric boundary layer. *Advances in Geophysics.*, Vol. 18A, Academic Press, 183–211.

Zeman, O., and J. L. Lumley, 1976: Modeling buoyance-driven mixed layers. *J. Atmos Sci.*, **33**, 1974–1988.

——, and H. Tennekes, 1977: Parameterization of the turbulent energy budget at the top of the daytime atmospheric boundary layer. *J. Atmos. Sci.*, **34**, 111–123.